Supporting Information

Metal-Doped Co_9S_8/MXene Nanocomposites for High-performance Electrochemical Capacitor Electrode Materials

Qun Yang[a,1], Yuan Ji[a,1], Wei Zhang[b], Fan Li[b], Min Zhou[b], Lina Ma[b], Jidong Dong[c*], Zaixing Jiang[a*]*

[a] *MIIT Key Laboratory of Critical Materials Technology for New Energy Conversion and Storage, State Key Laboratory of Urban Water Resource and Environment, School of Chemistry and Chemical Engineering, Harbin Institute of Technology, Harbin 150001, P. R. China.*

[b] *College of Chemistry and Chemical Engineering, Qingdao University, Qingdao 266071, P. R. China.*

[c] *Material Science and Engineering College, Northeast Forestry University, Harbin 150040, P. R. China.*

* Corresponding author:

E-mail address: malina@qdu. edu. cn (L. N. Ma)

dongjidong1122@126. com (J. D. Dong)

jiangzaixing@hit. edu. cn (Z. X. Jiang)

1. Experimental section

1.1 Chemicals

Cobalt chloride hexahydrate ($CoCl_2·6H_2O$), Aluminum chloride hexahydrate ($AlCl_3·6H_2O$), Cobalt sulfate heptahydrate ($CoSO_4·7H_2O$), Ferrous sulfate heptahydrate（$FeSO_4·7H_2O$）and Potassium hydroxide(KOH) were purchased from McLean Biochemical Technology Co. LTD. Ethylene glycol, N, N-dimethylformamide and thiourea were applied from Aladdin Industrial Corporation. All the chemicals were used without further purification.

1.2 Syntheses of Al-Co_9S_8/MXene nanocomposite

The preparation processes for Al-Co_9S_8/MXene as follows. 60 mg of obtained MXene powder was added to a mixed solution comprising 6 ml of ethylene glycol and 24 ml of N, N-dimethylformamide. After ultrasonication for 25 minutes, the mixture was mixed with $CoCl_2·6H_2O$ (1.4mmol,0.334g) and $AlCl_3·6H_2O$ (0.2mmol,0.048g) and stirred for 15 minutes, then added thioureas (4.2mmol,319.7mg) and stirred for 30 minutes. The resulting mixture was transferred to a Teflon autoclave, heating to 160℃ at a warming rate of five degrees per minute and holding for 12 hours. The resulting products were removed and centrifuged three times at 10500rpm with ethanol and deionized water for 15 minutes each time, finally, the obtained powder was subjected to a freeze-drying process lasting 20 hours to obtain the Al-Co_9S_8/MXene composites.

1.3 Synthesis of Fe-Co_9S_8/MXene nanocomposite

The synthesis procedure for Fe-Co_9S_8/MXene closely mirrors that of Al-Co_9S_8/MXene, with the sole difference being the substitution of $CoCl_2·6H_2O$ and $AlCl_3·6H_2O$. In this case, $CoSO_4·7H_2O$ (1.4 mmol, 0.393 g) and $FeSO_4·7H_2O$ (0.2 mmol, 0.056 g) were used. All other conditions and steps remain consistent with those employed for Al-Co_9S_8/MXene.

1.4 Characterization

The images of scanning electron microscopy (SEM) and Energy Dispersive X-ray Spectroscopy (EDS) were acquired from FE-SEM (SU8010). The information on lattice and Selected Area Electron Diffraction (SAED) was derived from Transmission Electron Microscopy (TEM, JEM-2100). The aperture distribution and type were obtained by Brunauer Emmett Teller (BET, Autosorb IQ MP) in a nitrogen atmosphere.

The X-ray Photoelectron Spectroscopy (XPS) and The X-ray powder diffraction (XRD) data were collected using an AXISULTRA DLD spectrometer and X PERT POWEDR, respectively.

1.5 Electrochemical measurements

The electrochemical tests were conducted by utilizing an electrochemical workstation (CHI 760e, China) at 6M KOH. The three-electrode system constructs from a working electrode, reference electrode (Hg/HgO), and counter electrode (platinum wire), To prepare the working electrode, nickel foam was initially cut into 1 cm x 1 cm pieces and then subjected to a 15-minute treatment with 3M hydrochloric acid, acetone, anhydrous ethanol and deionized water using ultrasound.

The slurry was then prepared, which was obtained by grinding with 80 wt% samples (Co_9S_8/MXene, Fe-Co_9S_8/MXene, and Al-Co_9S_8/MXene), 10 wt% activated carbon as a conducting agent, 10 wt% Polytetrafluoroethylene (PTFE) and anhydrous ethanol. This slurry was coated onto nickel foam and dried in a vacuum oven at 80℃ for 6 hours. The loadings of active substances in this paper are all around 1 mg. The range of electrochemical impedance spectroscopy (EIS) is from 0.01-100000Hz, and the voltage ranges of cyclic voltammetry (CV) and galvanostatic charge-discharge (GCD) are from 0 to 0.45V. Significantly, the specific capacitance Cm can be estimated from GCD through the following equation:

$$C_m = \frac{I \times \Delta t}{m \times \Delta V} \quad (1)$$

Where I (A) refers to current density, Δt (s) represents discharge time, m (g) expresses electrode mass, and (V) is the potential window.

1.6 Capacitance analysis

The real C′(ω) is associated with the complex impedance Z(ω) and its imaginary part $Z''(\omega)$, in contrast to the imaginary C″ (ω) is derived from the complex impedance Z(ω) and its real part $Z''(\omega)$:

$$C^{'}(\omega) = -Z''(\omega)/(\omega|Z(\omega)|^2) \quad (2)$$

$$C^{''}(\omega) = -Z'(\omega)/(\omega|Z(\omega)|^2) \quad (3)$$

Where ω represents the angular frequency, and the relaxation time constant can be calculated from the equation $\tau_0=1/f_0$, where f_0 denotes the frequency.

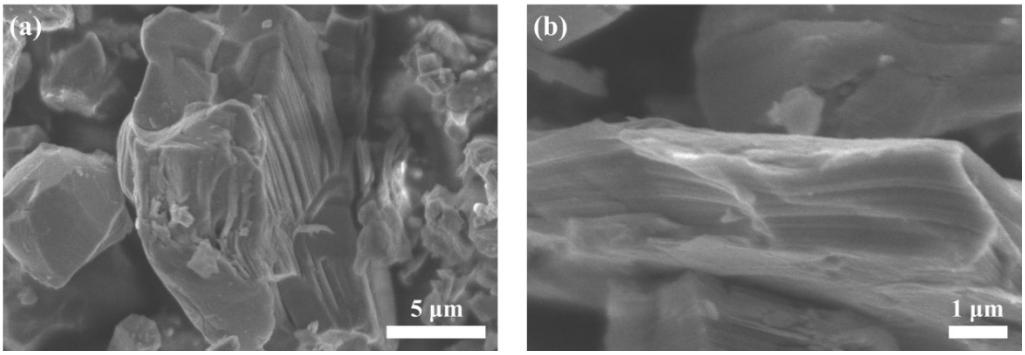

Fig. S1. SEM images of MXene

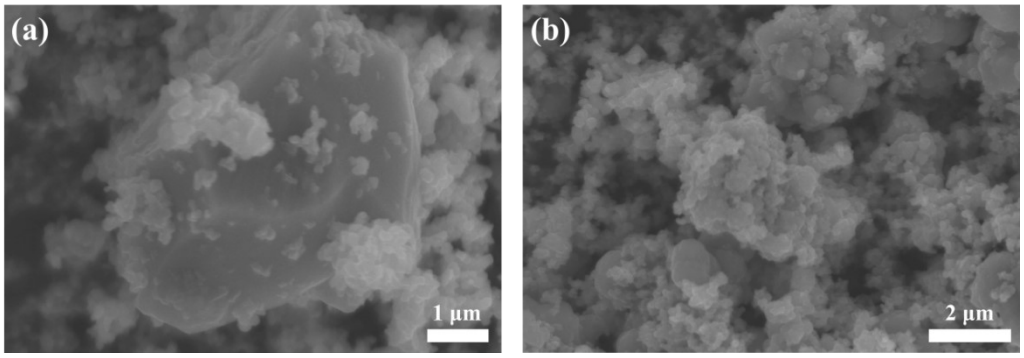

Fig. S2. SEM images of Co_9S_8/MXene

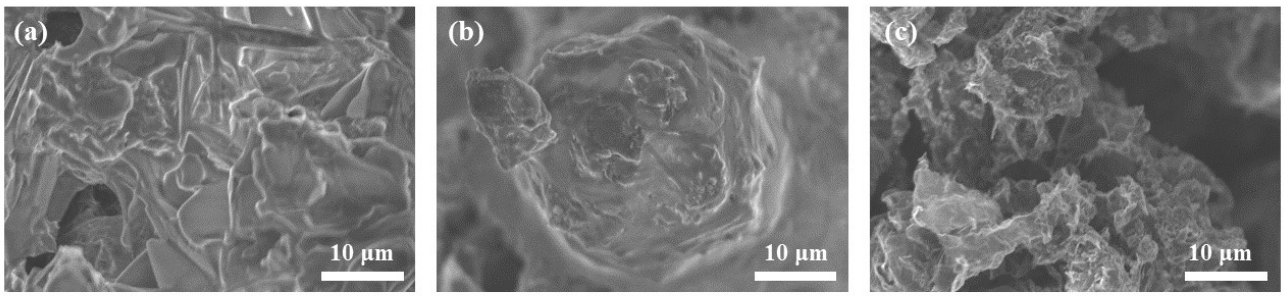

Fig. S3. SEM images after cycling of (a) Al-Co_9S_8/MXene (b) Fe-Co_9S_8/MXene (c) Co_9S_8/MXene

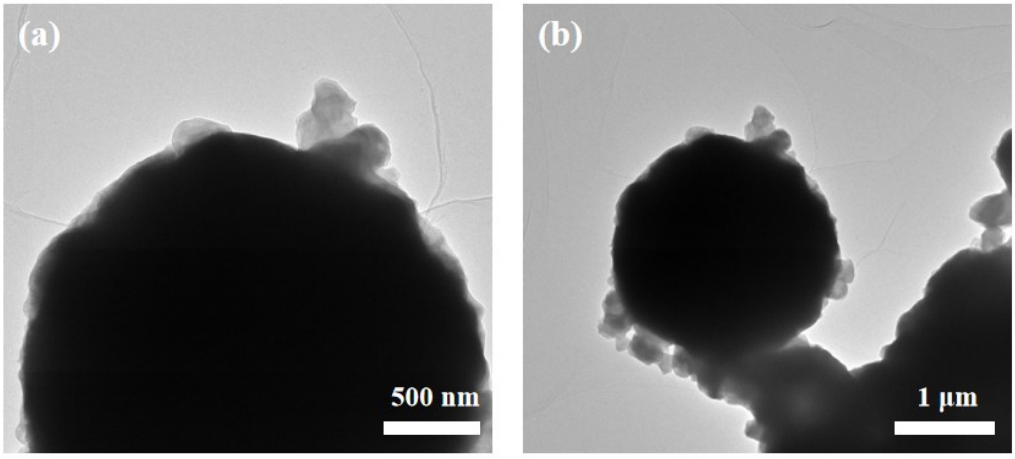

Fig. S4. TEM images of Al-Co_9S_8/MXene

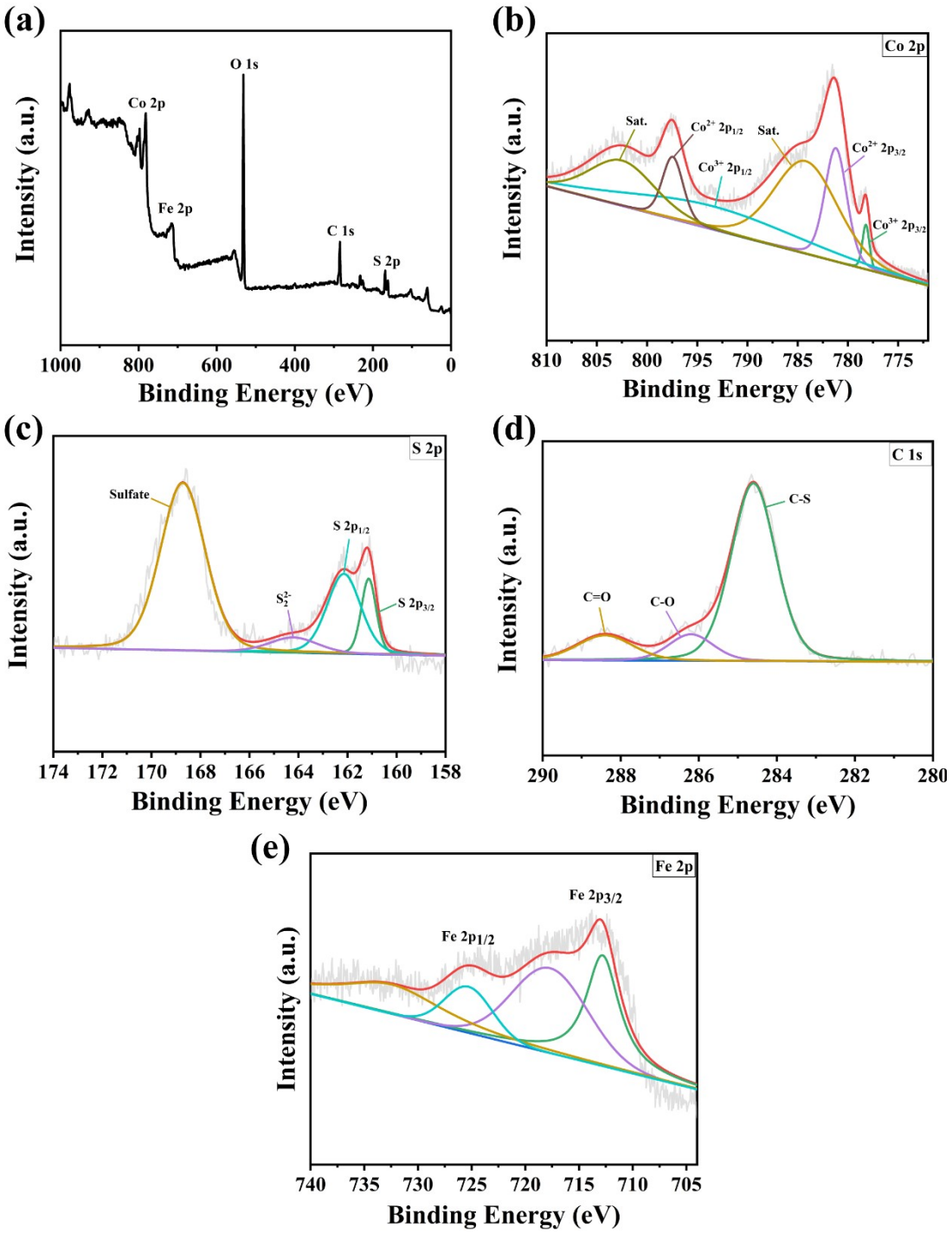

Fig. S5. (a) Full XPS pattern, high-resolution XPS spectra for (b) Co 2p (c) S 2p (d) C 1s (e) Fe 2p of Fe-Co_9S_8/MXene

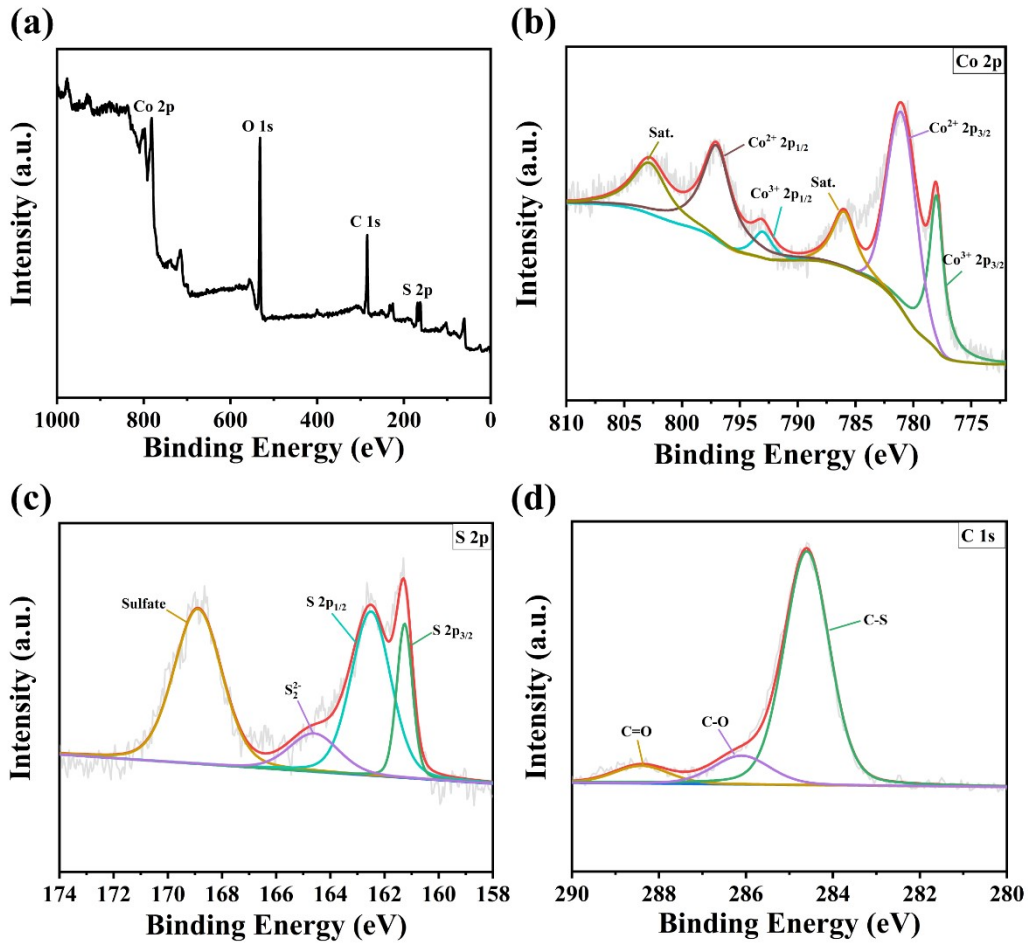

Fig. S6. (a) Full XPS pattern, high-resolution XPS spectra for (b) Co 2p (c) S 2p (d) C 1s of Co_9S_8/MXene

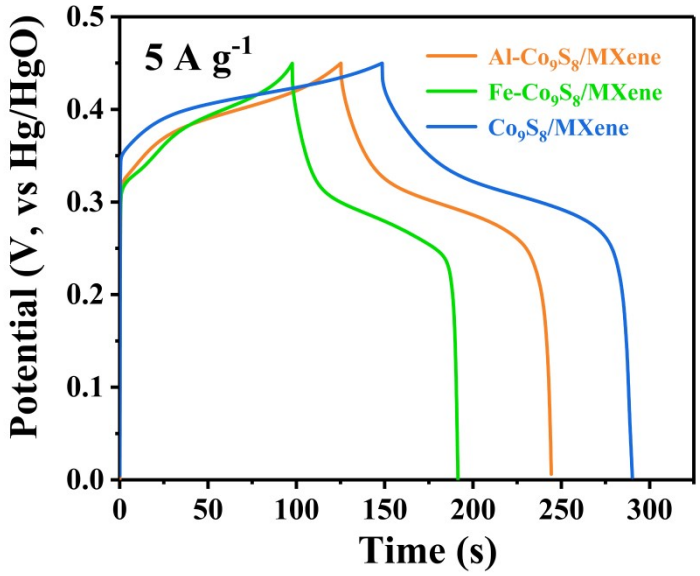

Fig. S7. GCD curves at 5 A g^{-1}

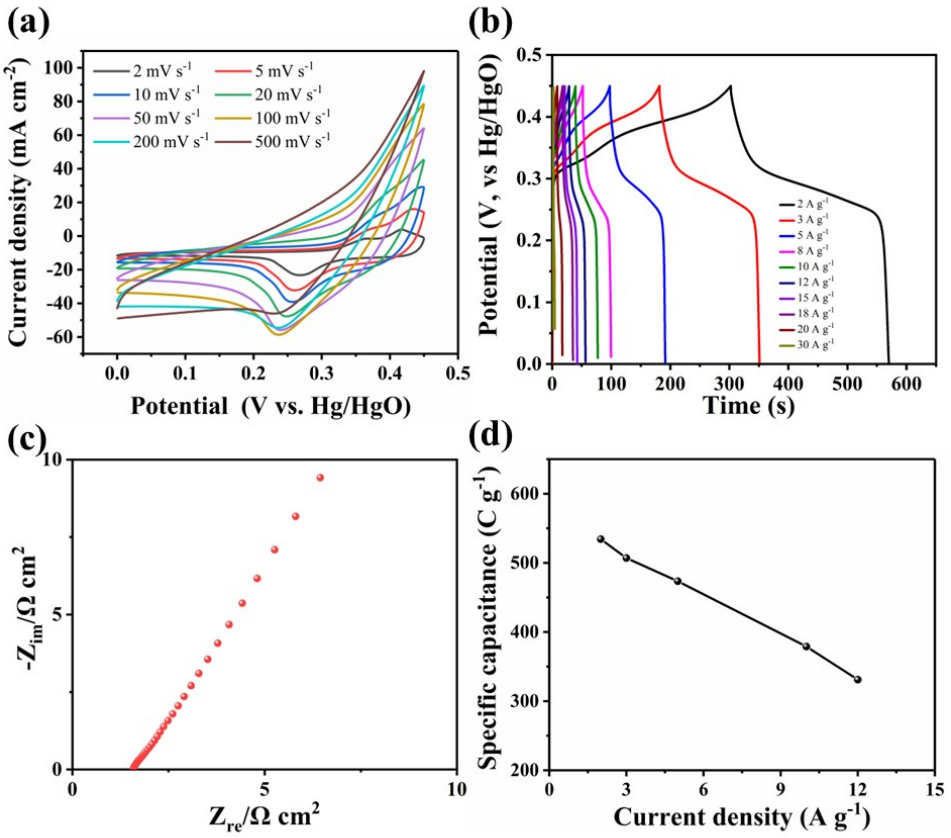

Fig. S8. (a) CV curves (b) GCD curves (c) Nyquist plots (d) Specific capacitance of Fe-Co_9S_8/MXene

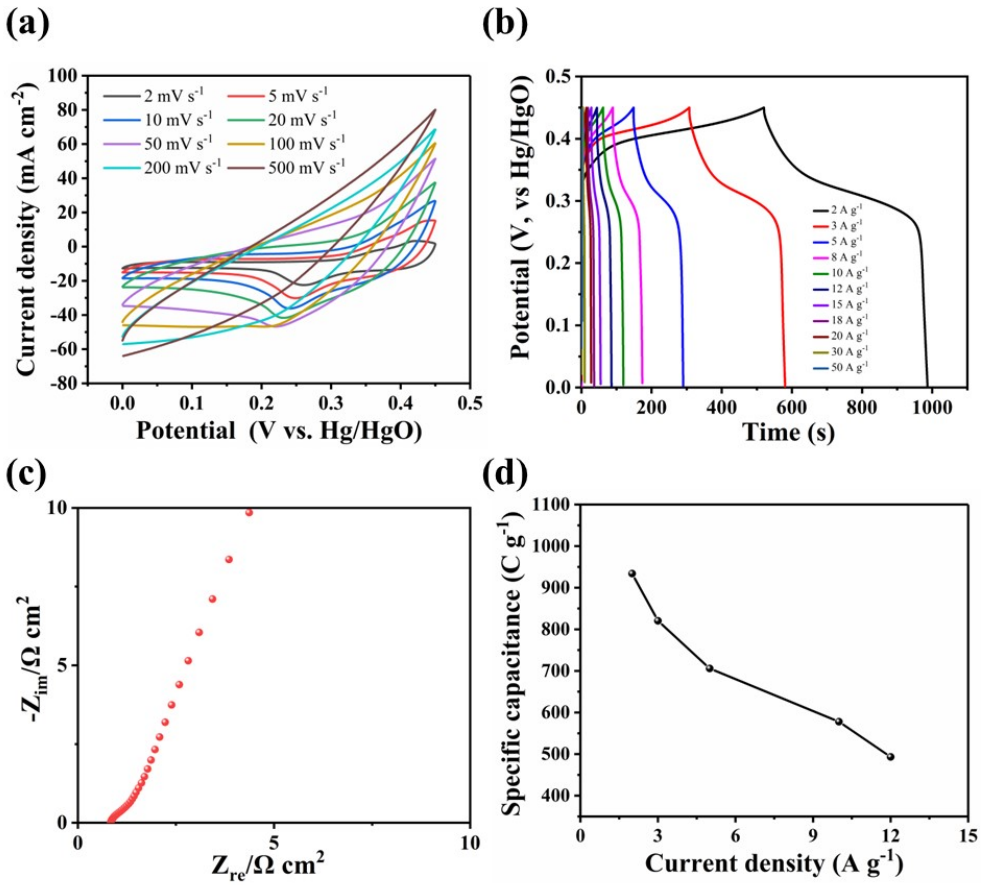

Fig. S9. (a) CV curves (b) GCD curves (c) Nyquist plots (d) Specific capacitance of Co_9S_8/MXene

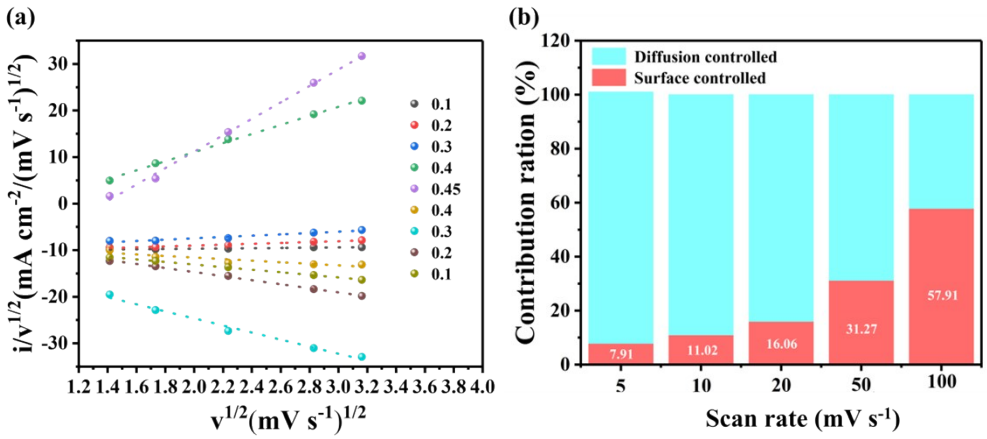

Fig. S10. (a) Current response to the square root of the scan rate versus the square root of the scan rate calculated from a positive scan. (b) Histogram showing the proportions of the surface-controlled capacitive contribution versus the scan rate.

Table S1. The literature on Metal oxide composites and metal sulfide composites electrodes.

Electrode	Electrolyte	Gravimetric capacitance ($F\ g^{-1}$)	Areal Capacitance ($F\ cm^{-2}$)	Potential range (V)	Capacitance Retention	Ref
Al-Co_9S_8/MXene	6 M KOH	1657.33 $F\ g^{-1}$ (2 $A\ g^{-1}$)		0.0-0.45	75% (2-12 $A\ g^{-1}$)	**Our work**
CoS	3 M NaOH	632 $F\ g^{-1}$ (1 $A\ g^{-1}$)		0.0-0.4	89.24% (1-20 $A\ g^{-1}$)	1
SnNiCoS	6 M KOH		18.6 $F\ cm^{-2}$ (5 $mA\ cm^{-2}$)	0.0-0.6	70.6% (5-30 $mA\ cm^{-2}$)	2
$NiCo_2S_4$/NF	2 M KOH	3093 $F\ g^{-1}$ (5 $A\ g^{-1}$)		0.0-0.4	68.8% (5-30 $A\ g^{-1}$)	3
$CoNi_2S_4$	6 M KOH	1136.5 $F\ g^{-1}$ (2 $A\ g^{-1}$)		0.0-0.4	38.58% (2-15 $A\ g^{-1}$)	4
$NiCo_2S_4$@CoS_2	2 M KOH	1565 $F\ g^{-1}$ (1 $A\ g^{-1}$)		0.0-0.55	27.5% (1-3 $A\ g^{-1}$)	5
Co_2CuS_4	6 M KOH	1005 $F\ g^{-1}$ (1 $A\ g^{-1}$)		0.0-0.5	76.6% (1-50 $A\ g^{-1}$)	6
$Zn_{0.76}Co_{0.24}S$	1 M KOH	486 $F\ g^{-1}$ (2 $A\ g^{-1}$)		0.0-0.45	77.6% (2-20 $A\ g^{-1}$)	7
Co_9S_8@$NiCo_2O_4$	3 M KOH	1966 $F\ g^{-1}$ (1 $A\ g^{-1}$)		0.0-0.5	81% (1-10 $A\ g^{-1}$)	8
$NiMoO_4$@CoCH/CC	1 M KOH		4.00 $F\ cm^{-2}$ (1 $mA\ cm^{-2}$)	0.0-0.45	62.5% (1-50 $mA\ cm^{-2}$)	9
FeS_2/PVP/NF	3 M KOH	526.08 $F\ g^{-1}$ (1 $A\ g^{-1}$)		0.0-0.5	57.8% (1-6 $A\ g^{-1}$)	10
VS_2	1 M KOH	2200 $F\ g^{-1}$ (1 $A\ g^{-1}$)		0.0-0.4	58% (1-10 $A\ g^{-1}$)	11
Ni_3S_4/CuS_2	1 M KOH	888 $F\ g^{-1}$ (1 $A\ g^{-1}$)		0.0-0.5	60.81% (1-10 $A\ g^{-1}$)	12
ZnS:Mn-NS	3 M KOH	1905 $F\ g^{-1}$ (1 $A\ g^{-1}$)		0.0-0.4	36.7% (1-20 $A\ g^{-1}$)	13
$CoMoS_4$@Ni-Co-S	3 M KOH	2208.5 $F\ g^{-1}$ (1 $A\ g^{-1}$)		0.0-0.4	68.8% (1-20 $A\ g^{-1}$)	14
Fe_7S_8@$Fe_5Ni_4S_8$	6 M KOH	670.4 $C\ g^{-1}$ (1$A\ g^{-1}$)		0.0-0.6	79.2% (1-20 $A\ g^{-1}$)	15

Reference

1. Y. C. Zhao, Z. Shi, H. Y. Li and C. A. Wang, *J. Mater. Chem. A*, 2018, **6**, 12782-12793.
2. T. T. Dai, B. Cai, X. J. Yang, Y. Jiang, L. Y. Wang, J. S. Wang, X. S. Li and W. Lü, *Nanotechnology*, 2023, **34**(22), 225401.
3. S. Wang, P. Zhang and C. Liu, *Colloids Surf. A Physicochem. Eng. Aspects*, 2021, **616**, 126334.
4. C. Jing, X. L. Guo, L. H. Xia, Y. X. Chen, X. Wang, X. Y. Liu, B. Q. Dong, F. Dong, S. C. Li and Y. X. Zhang, *Chem. Eng. J.*, 2020, **379**, 122305.
5. M. Govindasamy, S. Shanthi, E. Elaiyappillai, S. F. Wang, P. M. Johnson, H. Ikeda, Y. Hayakawa, S. Ponnusamy and C. Muthamizhchelvan, *Electrochim. Acta*, 2019, **293**, 328-337.
6. M. Guo, J. Balamurugan, T. D. Thanh, N. H. Kim and J. H. Lee, *J. Mater. Chem. A*, 2016, **4**, 17560-17571.
7. J. Yang, Y. Zhang, C. C. Sun, G. L. Guo, W. P. Sun, W. Huang, Q. Y. Yan and X. C. Dong, *J. Mater. Chem. A*, 2015, **3**, 11462-11470.
8. Q. Liu, X. D. Hong, X. Zhang, W. Wang, W. X. Guo, X. Y. Liu and M. D. Ye, *Chem. Eng. J.*, 2019, **356**, 985-993.
9. F. F. Wang, K. Ma, W. Tian, J. C. Dong, H. Han, H. P. Wang, K. Deng, H. R. Yue, Y. X. Zhang, W. Jiang and J. Y. Ji, *J. Mater. Chem. A*, 2019, **7**, 19589-19596.
10. I. K. Durga, S. S. Rao, R. M. N. Kalla, J. W. Ahn and H. J. Kim, *J. Energy Storage*, 2020, **28**, 101216.
11. Z. L. Guo, L. Yang, W. Wang, L. X. Cao and B. H. Dong, *J. Mater. Chem. A*, 2018, **6**, 14681-14688.
12. Y. Z. He, X. L. Zhang, S. T. Wang, J. X. Meng, Y. W. Sui, F. X. Wei, J. Q. Qi, Q. K. Meng, Y. J. Ren and D. D. Zhuang, *J. Alloys Compd.*, 2020, **847**, 156312.
13. I. Hussain, D. Mohapatra, G. Dhakal, C. Lamiel, S. G. Mohamed, M. S. Sayed and J. J. Shim, *J. Energy Storage*, 2020, **32**, 101767.
14. F. Ma, X. Q. Dai, J. Jin, N. Tie and Y. T. Dai, *Electrochim. Acta*, 2020, **331**, 135459.
15. M. M. Zhang, H. Liu, Y. Wang and T. J. Ma, *J. Colloid Interface Sci.*, 2019, **536**, 609-617.